ICAST2014 #063

A FBG Strain-Angle Transducer for Multi Body Morphing Rib Architecture: Conceptual Design and Numerical Modelling

G. Amendola[1*], M. Ciminello[1], I. Dimino[1], S. Ameduri[1]

[1] Smart Structures and Vibro-acoustics Laboratory, Centro Italiano Ricerche Aerospaziali, Capua (CE), Italy

Abstract

The object of this work is the conceptual design and modelling of a sensor based on Fiber Optic technology and conceived to measure rotations of rigid components around a pivot. The device, namely PB-FBG, is constituted of a flexible plate integrated with a FBG sensor; the edges of the plates are hinged onto the rotating rigid bodies, eccentrically with respect the pivot. In this way, any increase of rotation produces a further bending of the plate corresponding to an FBG wavelength shift.

Among the different applications, an aileron morphing architecture is considered. This architecture is made of a rib split into three rigid parts, hinged each other and moved through a dedicated kinematic chain. Two PB-FBG devices are installed between the adjacent rib blocks and give a measure of their current angular rotation. A peculiarity of the proposed device is its ability in working in post-buckling configuration, with two main advantages: 1) easy, plug and play, installation (the device supporting plate can be manually bent and plugged within the connection hinges); 2) tuning of the sensitivity / range of measure, on the basis of the FBG location onto the plate and of the initial post-buckling level.

At first the conceptual design was dealt with: a theoretical model describing the post buckling behaviour of beams was implemented, highlighting the effect of the main design parameters (e.g. length of the plate, thickness, width, material) on the achieved displacement/deformation; then, the plate displacement field was related to rotation angle of the rib parts around the pivots; a dedicated numerical (FE) model was thus realized to prove the concept feasibility and to simulate in detail its functionality. Finally, an installation layout was developed meeting criteria of lightness, small invasiveness, simplicity and limited costs.

[*] g.amendola@cira.it

1. INTRODUCTION

Modern aircraft possess many advanced functions, such as good transportation capability, high Mach number, high flight altitude and increasing rate of climb. However no aircraft has possibility to reach all of this optimized performance in a single airframe configuration. The aircraft aerodynamic efficiency vary considerably depending on specific mission and on environmental conditions within which the aircraft must operate. An aircraft design that is optimized for a single design point, which is the point of minimum drag, implies that its aerodynamic performance would degrade when leaving its ideal flight condition [1]. As a result, aircraft wings suffer large off-design performance penalties and different shapes may be needed under different operating conditions. In the view of improving aircraft performance, a concept that is more and more gaining space in the future aircraft design perspectives, is morphing wing. In aeronautics morphing is associated with adaptive wing shape modifications aiming to increase adaptability in flight regimes as well as innovative functionalities.
Standing the current knowledge, such morphing capabilities can only be achieved by the use of dedicated kinematics, [2], that can match the inconsistent requirements of systems, called to exhibit large displacements while preserving the capability of bearing external loads within confined strains.

Figure 1. Biologically inspired morphing aircraft: sliding skin (Raytheon, sweep angle changes) [3]

Examples of precursors in developing biologically inspired morphing aircraft include the AFTI/F-111 MAW with its variable camber wing [4], the AAW with twist control [5] and NASA's HECS wing [6]. In all these attempts, the morphing aircraft exhibit tunable aerodynamic properties to suit the needs of multi mission roles, having in common the objective of realizing wings that can accommodate the variations occurring during a typical mission or, either, between mission and mission, by changing their shape. The necessity of guaranteeing continuous external smooth surface smart skins in turns have to undergo large deformations (Figure 2) in turn linked to large strains (more than 5%) [7].

Among the most recent funded programs devoted to that topic is the Clean Sky - JTI launched by the EC in the FP8. In particular the "Low Noise Configuration" project within JTI pursues, address technology innovation for a next generation aircraft for highly-efficient aerodynamics, to reduce fuel consumption and pollution at cruise condition by the design of a morphing airfoil [8]. The innovative architectural design, on which the morphing capability is experienced, is based on a multi-block rib system, each activated by rod-like load-bearing actuators (Figure 2).

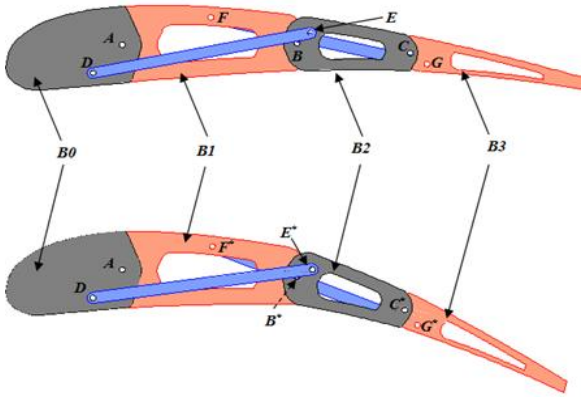

Figure 2. JTI-GRA: multi-block rib system.

Another example of European massive cluster devoted to this topic is the SARISTU Project, sponsored by the EU inside the VII Research Framework Program, [9] focusing, on Smart Intelligent Aircraft Structures. One of the target is the design and realization of an ATE device [1]. Chord and span-wise ATED camber variations may allow setting and chasing the best lay-out as a function of the particular and transforming reference state, always targeting best aerodynamic and structural performance. Key aspects are architectural layout definition, development of a suitable skin (longitudinally deformable but transversely rigid), shape control system assuring the specified displacement tolerances.

A more recent ongoing research project, leaded by the Consortium for Research and Innovation in Aerospace in Quebec (CRIAQ), is currently working on a prototype of a real scale outer wing of a regional aircraft consisting of a morphing wing and variable-camber aileron designed, fabricated and tested. Wind tunnel data analysis will be performed to assess the effectiveness of the aerodynamic performances of the entire system, in particular there will be a comparison between the aerodynamic characteristics measured from the conventional aileron and the morphed one. The upper surface of the wing box will be equipped with a flexible composite skin. Electrical motors driven actuators will act on the inners skin surface in order to change airfoil thickness for better aerodynamic performances. The aileron will be morphed using a set of servo rotary actuators distributed along the aileron span as integral parts of the structure [11]. A preliminary structural layout will also be presented in this paper referring however to the aileron rib (shown in Figure 3 with sensor supporting hinges A,B,C and D) for calculation. Particularly, in order to ensure both the controllable and the static robustness of these complex structural systems, a monitoring networks is needed aimed at verifying the effectiveness of the given control commands together with the elastic response under the external aerodynamics and mechanical loads. In order to achieve this kind of information, the use of an original FBG strain-angle network transducer for morphing aileron rotation is, in this work, proposed.

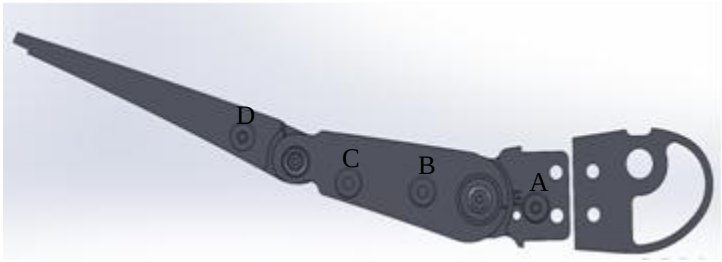

Figure 3. CRIAQ: multi-body rib.

The reason why an optical sensor solution has been selected arose from the consideration that many of the most common angular/rotary devices are typically wired sensors requiring supply voltage, supply current, packaging type, processing unit for analog/digital output. The most common values for supply voltage are 4.5 to 5.5 V. Supply current can have a range between 100 μA and 13.5 A, with the most common chips having a supply current of 13.5 mA. Nevertheless the above mentioned wired sensors, may bring to improbable or impracticable architectures and sometimes their physical dimensions cannot fit the available space inside the structure to be monitored.
On the other side, while keeping a few of the contraindication of the classical systems (like cabling, continuous deployment, and so on), fibre optic sensors may lead to a dramatic improvement of the channels number and the wiring needs, above all thanks to an extreme multiplexing capability [12][13][14][15][16][17]. Furthermore, the use of the "light" as "information carrier", permits dealing with nimbler, non-shielded wires and avoids any kind of interference with the on-board instrumentation, confining to the laser sources and other similar electronic equipment the unavoidable certification issues. The innovative FBG-based sensor system aims at monitoring the actual shape of morphing ribs because aerodynamic benefits related to the morphing structures, are very sensitive to the actual wing shapes achieved during the aircraft mission. Compared to conventional rotational sensors which may be namely embedded into the morphing ribs kinematics, this concept allows a more distributed assessment of the wing camber variation by taking advantage of a supporting structure hosting FBG sensors. In addition, the supporting structure acts as a strain modulator whose properties may be tailored depending on the architectural requirements and structural constraints.

However direct strain measurement may be difficult because of the large deformations, usually occurring in morphing structures are much larger than the standard fibres can handle (usually, up to 2%). In recent years, the use of optical fiber sensors modulations for high deformations monitoring has become an interesting topic [18]. A modulation transducer is then necessary to keep the measured strain inside the allowed range. In this specific application, the transducer device is made of a clamped-clamped post-buckled beam coupled to the monitored component. FBG sensors are integrated along the path of the beam. The FBG position along the path can be almost arbitrarily set in order to measure a large range of strain values.

In what follows, the geometry of the concept and the selected sensor are described for an isotropic beam material. A theoretical model describing the post buckling behaviour of beams is implemented, highlighting the effect of the main design parameters (e.g. length of the plate, thickness, width, material) on the achieved displacement/deformation; then, the plate displacement field was related to rotation angle of the rib parts around the pivots. Then a dedicated numerical FE model was thus realized to prove the concept feasibility and to simulate in detail its functionality. Finally, an installation layout was developed meeting criteria of lightness, small invasiveness, simplicity and limited costs.

2. WORKING PRINCIPLES

An elastic post-buckling beam with a small cross section (negligible thickness with respect to the total length) is herein considered, so that it belongs to the class of slender curved beams [18]. When such a structure is subjected to a moment (around the pivot), it will further bend. The following hypotheses are made on the geometry and its material:

- Applied load around the symmetry point;
- Constant cross-section and homogeneous material;
- Inextensibility (symmetry axes preserved under deformation)→ Pure bending deformation

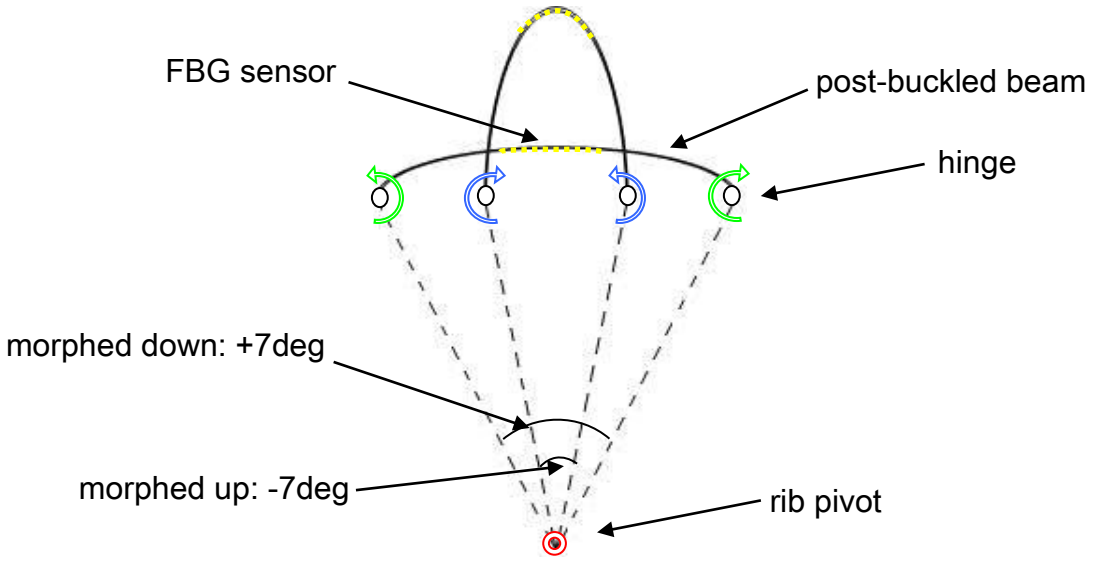

Figure 4. Conceptual scheme of the PB-FBG system.

The PB-FBG system is sensorized by using FO technology. The angular position of the FBG sensor along the beam neutral axes governs the ratio between the rib pivot rotation angle and the measured deformation, that can be then arbitrarily set in a very large range of values according to the beam local curvature. From Figure 4 the conceptual scheme of the device is illustrated. The rib pivot governs the multi body rib relative rotation. A post-buckled elastic beam is anchored to adjacent bodies of the rib by means of hinges allowing the beam to follow the rotation. According to the specific morphing configuration that can spread from -7deg of morphing up to +7deg of morphing down, the beam can experience a pure bending deformation. An FBG sensor is bonded on the surface of the beam and it is used to measure the local strain.
The flexible beam can be dimensioned according to the specific structural application without losing the modelling approach. A peculiarity of the proposed device is its ability in working in post-buckling configuration, with two main advantages: 1) easy, plug and play, installation (the device supporting plate can be manually bent and plugged within the connection hinges); 2) tuning of the sensitivity/range of measure, on the basis of the FBG location onto the plate and of the initial post-buckling level.

This concept belongs to the family of the strain modulators and the main innovation consists in the large modulation capability related to its peculiar geometry. Finally, the adoption of two collocated FBG (opposite side of the beam) can be used for self-compensated temperature measures, being, this arches subjected to the unsymmetrical stress loads but to the same temperature gradient.

3. THERETICAL MODELING

The system shown in the previous section was analytically described by [19]. The FBG supporting beam can be ideally split into two identical clamped beams (see Figure 5). Assuming the horizontal load F (representing the action of the hinges A and B of Figure 4), the bending moment onto the free edges is zero and the model described can be adopted.

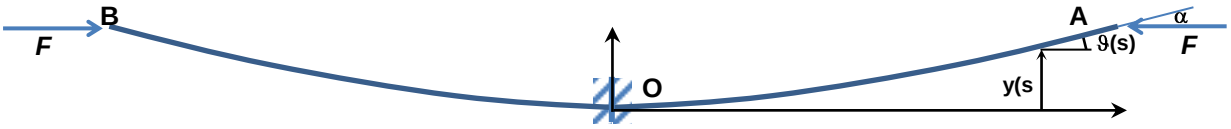

Figure 5. Theoretical structural scheme.

The beam equation, under the assumption of large displacements can be written as it follows:

$$EI\frac{d\vartheta}{ds} = -Fy\ \ s \qquad (1)$$

where E and I are the material Young modulus and the cross section inertia moment (assumed to be rectangular), s is the curvilinear abscissa and ϑ and y are the slope of "elastica" curve and the vertical displacement

These two terms are linked by the following differential relation

$$\frac{dy}{ds} = \sin\vartheta \qquad (2)$$

Deriving eq. (1) and substituting relation (2) to the derivative of y, the nonlinear (large displacement) pendulum equation can be finally obtained

$$EI\frac{d^2\vartheta}{ds^2} = -F\sin\vartheta \qquad (3)$$

This last equation describes the deformation of the beam in terms of ϑ and can be solved numerically or using the elliptic integrals tables. The following approach was used to solve eq (3) at different configurations:

- Since each configuration is univocally identified by the slope α of the curve at the free edge, this value is initially assigned
- The parameter $p = \sin\frac{\alpha}{2}$ is computed and the value **K**(p) of the complete elliptic integral of first kind is computed.
- as shown in [19], this value is related to the beam length, l, the Young moduli, E, the section inertia moment, I, and the applied force F by the relation

$$l = \boldsymbol{K}\ p\quad\overline{\frac{EI}{F}} \qquad (4)$$

- thus the value of the force F can be computed
- again in [19], the relations to compute the horizontal, x, and vertical, y displacements of the free edge are provided:

$$x_A = 2\ \ \overline{\frac{EI}{F}}\cdot\boldsymbol{E}\ p\ \ - l \qquad (5)$$

$$y_A = 2p\ \ \overline{\frac{EI}{F}} \qquad (6)$$

where ***E*** is the value of the complete elliptic integral of second kind.

- once identified the displacement of the free edge, being constant its distance from the pivot O, its rotation can be estimated
- finally also the curvature $\frac{d\vartheta}{ds}$ and, thus, the strain (times the half thickness *t* of the beam) at the FBG station can be computed by substituting in (1) the value found for F and the vertical displacement y_A

In the end, through this approach it is possible to link the rotation around the pivot O to the strain read by the FBG.
A dedicated model was implemented and used to identify the optimal compromise among the most relevant sensor parameters. In Figure 6, top, the FBG strain was related to two parameters: the initial angle around the pivot of the rib adjacent parts, namely Φ_0, and the distance of the beam hinges (A or B) from the pivot, namely *r*. The corresponding derivatives, representing the sensitivity of the sensor, were plotted on the bottom graph.
Observing these graphs, it is possible to distinguish different families of curves, each one corresponding to a specific initial value of Φ_0; thus, e.g., the second family of curves moving from the left side corresponds to an initial angle of about 68 deg. Each family is then constituted by 5 curves corresponding to increasing values of *r*, moving downward as shown by the arrow. Furthermore in the plot on the top also the maximum readable (allowable) strain from the FBG was depicted (dashed line). The configuration (Φ_0 and r) chosen for the next numerical investigations and taken into account for future practical realization (prototype manufacturing) was identified meeting the following criteria:

1. maximization of the sensitivity of device
2. achievement of a measurement (angle) range as wide as possible
3. structural integrity of the supporting beam and of the FBG
4. reduction of any interference with the aileron device functionality
5. integration within the available space

The optimal compromise among these aspects was highlighted through the bold lines in Figure 6. The corresponding angle and distances values are 178 deg and 33 mm, respectively and assure a sensitivity obtained is of 100 micro-strain per deg.
It is noteworthy that the measurement range (more than 18 deg) widely covers the aileron global deflection (± 7 deg), before arriving to the FBG limit (intersection of the curve with the dashed line). The other families of curves on the left, even though characterized by higher values of sensitivities (see bottom graph), were not considered because of the lower measurement range (lower distance between Φ_0 value and the crossing point with the dashed line). The optimal curve belonging to the selected family was eventually identified respecting the integration requirement (available room). The picked configuration, as it will be shown in the next section, is also characterized by an acceptable compliance with respect the aileron functionality (low elastic reaction due to the post-buckling working modality).

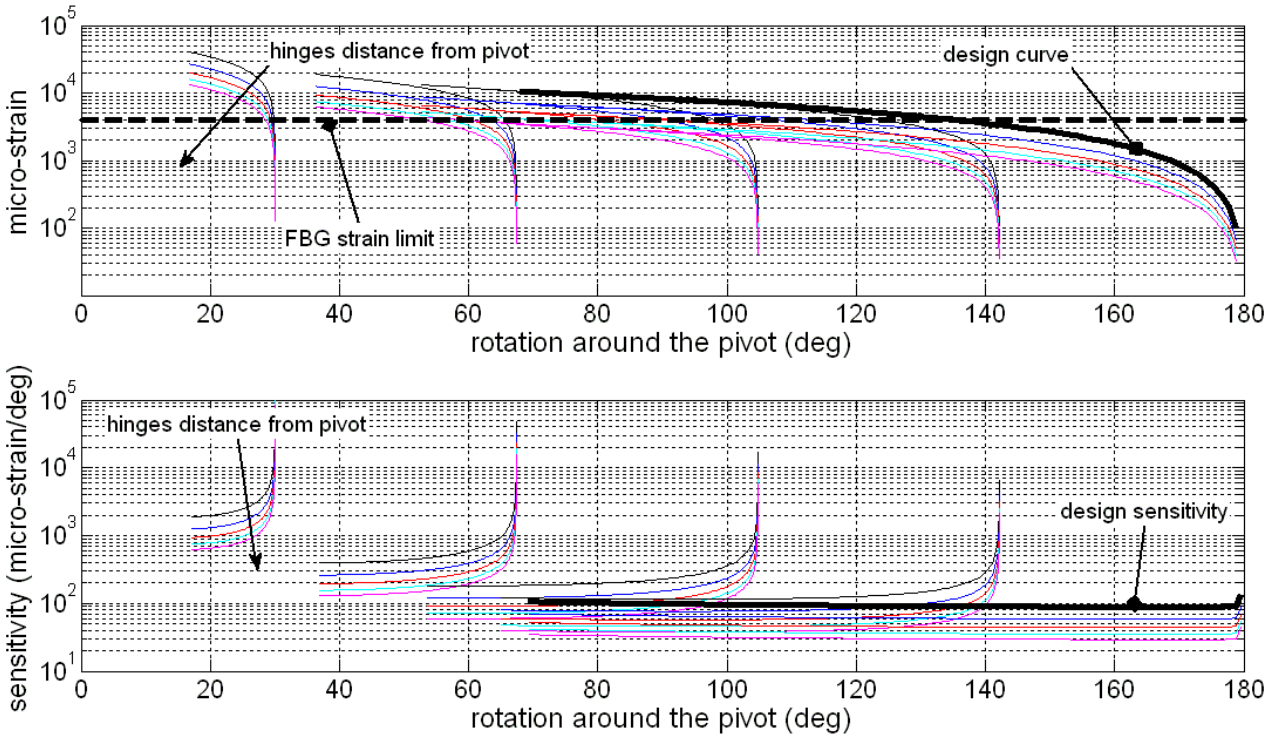

Figure 6. FBG strain vs. initial pivot angle vs. distance of the hinges from the pivot.

On the basis of this analytic model and exploiting the GUI capabilities of Matlab ®, a dedicated tool was implemented, enabling the geometric representation of the two movable rib blocks with respect to the deflection level of the sensor supporting beam. In Figure 7 a screen shot is depicted, reproducing the aileron in downward full activation; it is possible to compare such a configuration with the deformation (curvature) of the FBG sensors (green arcs).

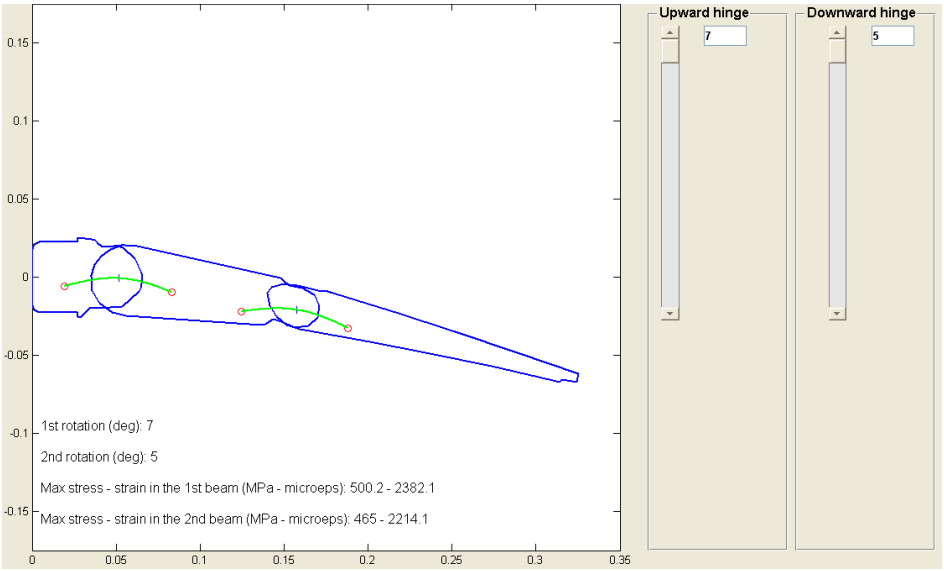

Figure 7. Matlab GUI tool for the graphical representation of the aileron deflection and of the corresponding deformation level of the FBG supporting beams (green).

4. FE MODEL

4.1 Beam conceptual numerical model

The aim of this section is to present the developed numerical model of the FBG supporting beam by means of FE analysis and to correlate the obtained results with the theory previously introduced. The beam model was realized with BAR2 finite elements, as shown in Figure 8 and the beam has a solid rectangular cross section with 0.3 mm of thickness and a depth of 10 mm.

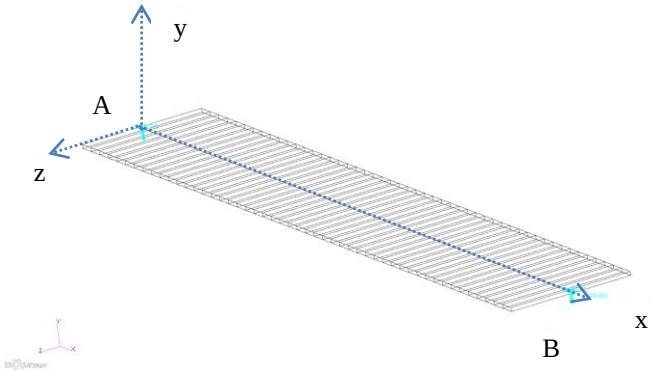

Figure 8. Beam FE model with nodal constraints.

In order to correctly estimate the beam post buckling behaviour buckling analysis has been firstly performed using MSC NASTRAN® solver (SOL 105). A compressive displacement of 10 mm, along the x direction, has been imposed to the hinge B while the point A was totally pinned. The resulting first order eigenvalue and the correspondent eigenvector are depicted in Figure 9.

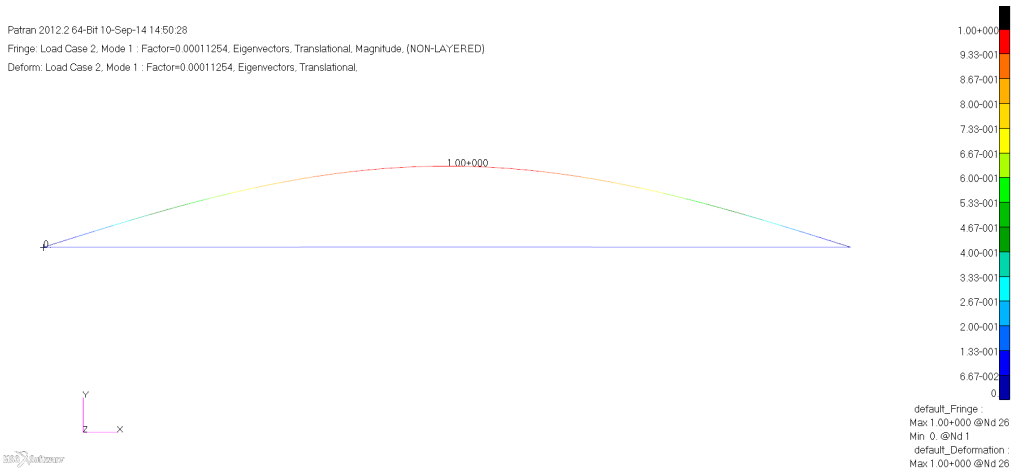

Figure 9. Beam buckling, 1st mode

The beam deformed shape was then scaled by the 3% of the cross section thickness in order to obtain the real deformation when external load reach the buckling value; this operation is justified by the fact that the instability is caused by a small asymmetry along the longitudinal axis; usually the surface roughness, of about 3% the thickness, may induce the instability. The new beam configuration (1st modal shape) was superimposed to the not deformed one giving to the structure an initial curvature which allows to characterize the post buckling behaviour. In light of this consideration a static nonlinear analysis was performed on the curved beam. The nodal displacements are reported in the next figure (Figure 10); moreover it is possible to relate the horizontal displacement of the point B (which represent the x_A abscissa in the analytic theory) with the vertical displacement of the node located in the middle of the beam (corresponding to y_A in the analytic theory).

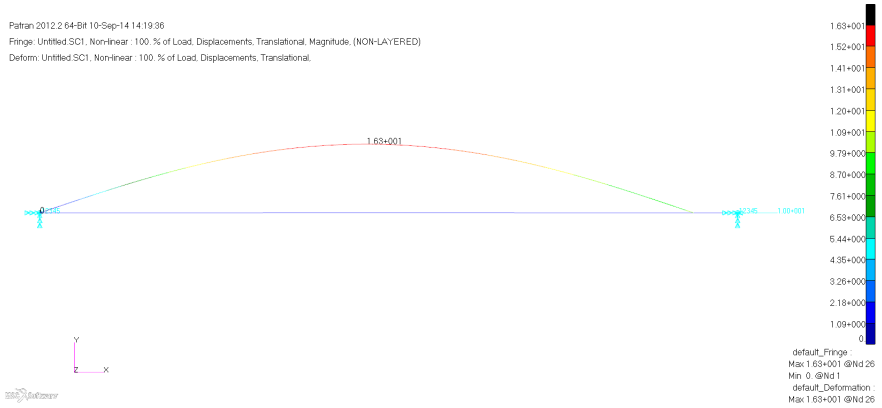

Figure 10. Beam deformation

Finally in the subsequent figure (Figure 11) a comparison between the displacements and the deformations obtained through the analytic and numeric approaches is given in terms of vertical displacement of the middle of the beam versus the horizontal displacement of the free edge; it is noteworthy that the two curves perfectly match.

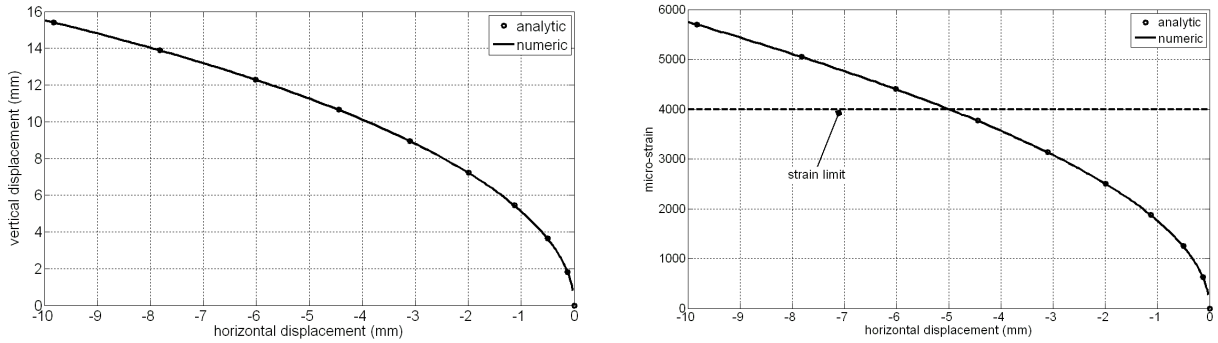

(a) (b)

Figure 10. Comparison between the analytic and the numeric model of the beam: vertical displacement (a) and strain (b) on the middle versus horizontal displacement of the free edge

5. SENSOR STRUCTURAL INTEGRATION LAYOUT

The concept above described was integrated within the aileron CAD and a hypothesis of layout was formulated. The CAD is representative of a real scale aileron for a regional aircraft. The morphing aileron is based on rigid-body mechanism which consist of a rib dived in several blocks or plates connected by means of hinges. In particular the leading edge is fixed while only two plates can deflect thanks to a dedicated single DOF actuation system driven by rotary servo actuators. The structure is then covered by a segmented aluminum skin with rubber gap fillers. The aileron structural layout is presented in Figure 11.

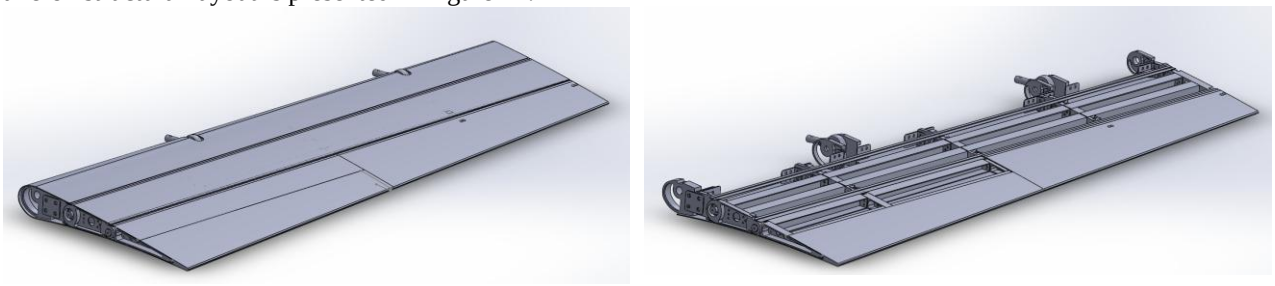

(a) (b)

Figure 11. CAD of the aileron: external view (a), inner architecture (b)

The sensor and the supporting beam were integrated in correspondence of the two hinges, as shown in Figure 12, depicting both the dimetric and the lateral view of the architecture.

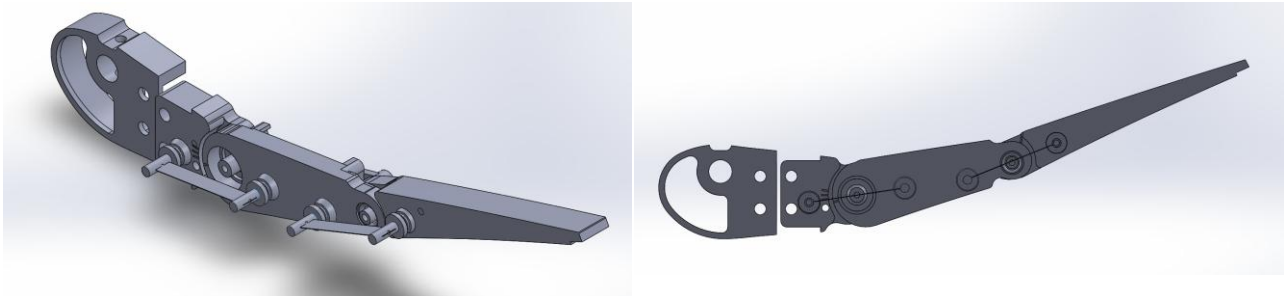

(a) (b)

Figure 12. Dimetric (a) and lateral (b) view of the aileron integrated with the sensor.

To assure the correct connection between the supporting beams and the rib blocks, that represent the pinned constraint condition, the set illustrated in Figure 13 was ideated.

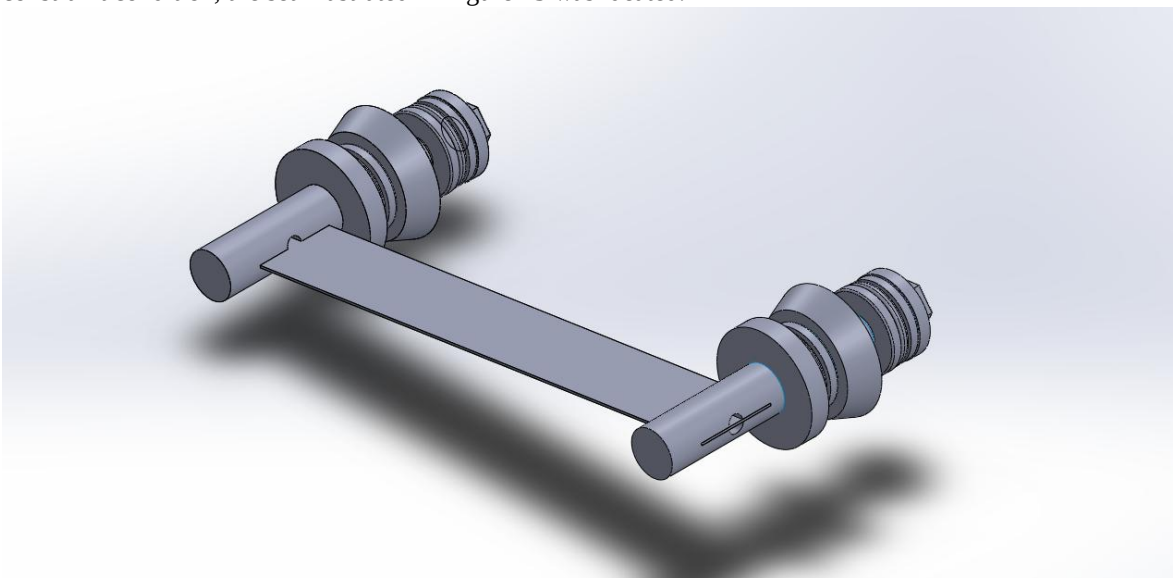

Figure 13. Set of connection between the sensor supporting beam and the rib part.

The set is in practice constituted by a pin with a groove at the external edge; note the hole in the groove, aimed to allow the fibre passing through it. The sensor supporting plate is integrated within this groove and any axial and radial translation is prevented through a clamping nut.
The pin constraint condition is assured by the two bearings integrated within the rib body, as shown in the cross section view of figure 14

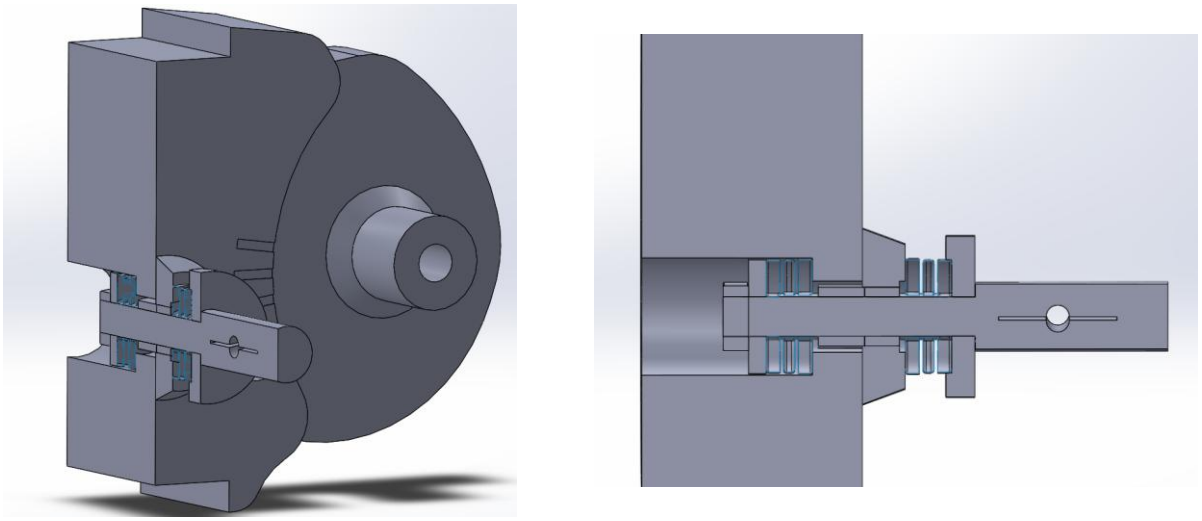

(a) (b)

Figure 14. Detail of the connection between the pin and the rib.

5.1 Sensor implementation

On the base of the analysis conducted in the previous section, a model of the beam (equipped with FBG sensor) connected to an hinge has been performed. The model aim to simulate the functional relation between rotation around pivot and the strain on the sensor. This is a representative situation of the operative functionality of the sensor when mounted on the aileron morphing rib, in fact the pivot represent the first rib hinge around which the rib plate can deflect during morphing. The beam model was simulated with BAR2 finite elements, as shown in Figure 15 (a) and the beam has a solid rectangular cross section with 0.3 mm of thickness and a depth of 10 mm. In order to model the rib morphing rotation, the hinge B was connected to the pivot through a more rigid linkage (solid cross section with 10 mm of thickness and a depth of 10 mm), in this way the rotation imposed to the pivot is transmitted to the post buckled beam geometry. At this point a non-linear static analysis has been performed with and imposed rotation of 1 rad (c.a. 57 degrees) at the pivot and the results obtain are reported in the Figure 15 (b). This rotation sweeps a very wide angle range but the morphing range from +/- 7 degrees covers only a limited portion. For this reason in the diagrams shown in Figure 15 (a) and (b) are reported the results for the design morphing deflection angles.

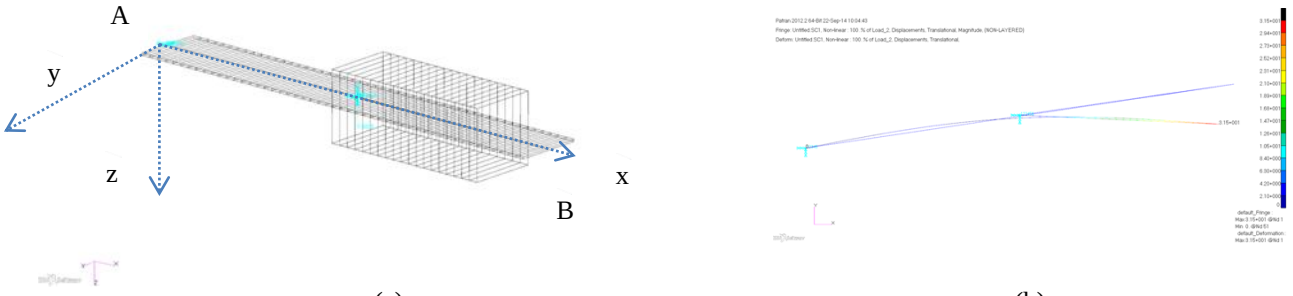

(a) (b)

Figure 15. Beam model (a) and deformation under a rotation of 57 degrees

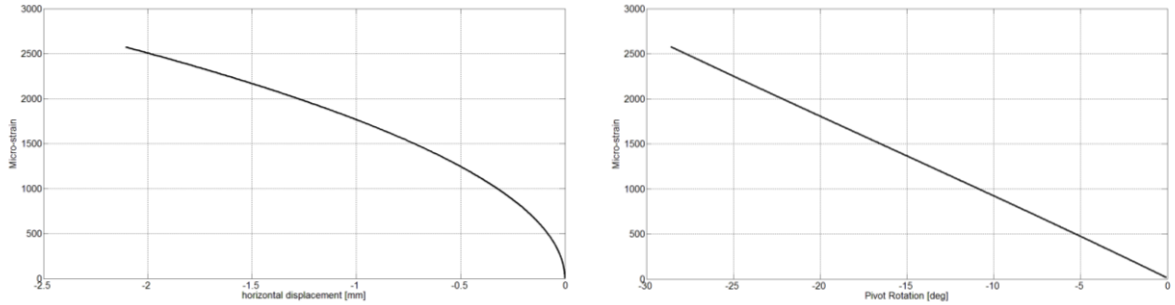

Figure 16. Horizontal displacement (a) and strain (b) calculated on the middle node of the beam versus rotation around pivot

6. CONCLUSIONS AND FURTHER STEPS

Morphing wing enables significant drag reductions in flight. However, its aerodynamic benefits are very sensitive to the actual wing shapes achieved during the aircraft mission. This papers details the feasibility study and a conceptual design of an innovative FBG-based sensor system aiming at monitoring the actual shape of morphing ribs. Compared to conventional rotational sensors which may be namely embedded into the morphing ribs kinematics, this concept allows a more distributed assessment of the wing camber variation by taking advantage of a supporting structure hosting FBG sensors. In addition, the supporting structure acts as a strain modulator whose properties may be tailored depending on the architectural requirements and structural constraints.
First, starting from the analytical model, a dedicated tool was implemented in order to optimise the sensor geometry while applied between two movable rib blocks. Then, the theoretical model was validated against FE trials.

In the design phase, the structural integrity of the supporting beam as well as its integration into the morphing structure were considered. The sensor system has been preliminary implemented into a morphing aileron aiming at controlling load distribution over the wing during flight. An operative hypothesis of structural layout was presented and integrated into the aileron CAD model.
Future steps of this work will involve a numerical correlation between the morphing rib deflections and the strain distribution over the FBG-based sensor system in order to validate the conceptual design. This will allow to associate the predicted morphing aileron conditions with the actual rib shapes, and, hence, to enable a more precise assessment of its enhanced aerodynamic performance and benefits.

ACKNOWLEDGMENTS

This work was developed within CRIAQ framework, a joint integration Project between Italian and Canadian research centres and industries.
Moreover, the authors would recall the precious contribution given by the Aerospace Division of the University of Naples "Federico II" for the aileron prototyping.

REFERENCES

[1] Seung-Hee Ko, Jae-Sung Bae and Jin-Ho Rho, Development of a morphing flap using shape memory alloy actuators: the aerodynamic characteristics of a morphing flap, Smart Materials and Structures, 2014

[2] I. Dimino, D. Flauto, G. Diodati, A. Concilio and R. Pecora, Actuation System Design for a Morphing Wing Trailing Edge, Recent Patents on Mechanical Engineering 2014, 7 (3): 138-148

[3] T. Weisshaar, "The next 100 years of flight—part two", NewScientist.com., News Service, December 2003.

[4] C.E.S. Cesnik, H.R. Last, C.A. Martin, A Framework for morphing capability assessment, in: Proceedings of the 45th AIAA/ASME/ASCE/AHS/ASC on Structures, Structural Dynamics&Materials Conference, Paper # AIAA 2004-1654, Palm Springs, CA, April 19–22, 2004.

[5] J.R. Wilson, Active aeroelastic wing: a new/old twist on flight, Aerospace Am. 40 (9) (2002) 34–37.

[6] J.B. Davidson, P. Chwalowski, B.S. Lazos, Flight dynamic simulation assessment of a morphable hyper-elliptic cambered span winged configuration, in: Proceedings of the AIAA on Atmospheric Flight Mechanics Conference and Exhibit, AIAA Paper 2003-5301, Austin, TX, August 11–14, 2003.

[7] J. Manzo, E. Garcia, A. Wickenheiser, G.C. Horner, Design of a shape memory alloy actuated macro-scale morphing aircraft mechanism, in: A.B. Flatau (Ed.), Proceedings of SPIE on Smart Structures and Materials 2005: Smart Structures and Integrated Systems, 5764, 2005, pp. 232–240.

[8] http://www.cleansky.eu/

[9] http://www.saristu.eu/project/activities/as-02-structural-tailoring-of-wing-trailing-edge-device/

[10] http://www.saristu.eu/wpcontent/uploads/2012/02/SARISTU-NEWSLETTER-Issue-01.pdf

[11] http://en.etsmtl.ca/Unites-de-recherche/LARCASE/Recherche-et-innovation/Projets
CRIAQ MDO-505 – Morphing Architectures and related technologies for wing efficiency improvement.

[12] Jones M. E., Duncan P. G., Crotts R., Shinpaugh K., Grace J. L., Murphy K. A. and Claus R. O., "Multiplexing optical fiber-based pressure sensors for smart wings", Proc. SPIE 2838 230–6.

[13] Stephan Rapp, Lae-Hyong Kang, Jae-Hung Han, Uwe C Mueller1 and Horst Baier1," Displacement field estimation for a two-dimensional structure using fiber Bragg grating sensors", Smart Mater. Struct. 18 (2009) 025006 (12pp)

[14] Duncan P. G., Jones M. E., Shinpaugh K. A., Poland S. H., Murphy K.A. and Claus R. O., "Optical fiber pressure sensors for adaptive wings", Proc. SPIE 3042 320–31.

[15] Xiao-Ming Tao et al. "Fiber strain sensor and measurement system for repeated large deformation", Patent N:US008276462B2, Date of Patent: Oct. 2, 2012

[16] Peter C. Chen, Shiping Chen "Fiber optic strain sensor" US 6668105 B2, Date of patent: 23 Dec 2003

[17] Falih H. Ahmad, James A. Evans, Barry D. Fehl, "Helical optical fiber strain sensor" US 5900556 A, Date of Patent: May. 4, 1999

[18] M. Ciminello, S. Ameduri, D. Flauto. Design of FBG based-on sensor device for large displacement deformation, IMOC2013, 4-7 August Rio de Janeiro. Proc. IEEE 113971.

[19] Timoshenko SP, Gere JM, "Theory of Elastic Stability", Mc Graw Hill International Book Company, 2nd Edition, pp.76-82.